Superlattice Intrinsic Stacking Faults in γ' Precipitates

Huis in't Veld, A.J.; Boom, G.; Bronsveld, P.M.; De Hosson, J.Th.M.

Published in:
Scripta Metallurgica

DOI:
10.1016/0036-9748(85)90021-3

Publication date:
1985

Scripta METALLURGICA Vol. 19, pp. 1123-1128, 1985 Pergamon Press Ltd.
Printed in the U.S.A.

Superlattice Intrinsic Stacking Faults in γ' Precipitates

A. J. Huis in't Veld, G. Boom, P. M. Bronsveld, J. Th. M. De Hosson

Department of Applied Physics, Materials Science Centre, University of Groningen, Nijenborgh 18, 9747 AG Groningen, The Netherlands.

(Received June 24, 1985)

1. Introduction

As a result of the advance in gas turbine engine-technology, new superalloys have found useful application because of their creep resistance at high temperature. The material properties of MA 6000 and other superalloys depend largely upon strengthening by $L1_2$ ordered γ' precipitates and to a lesser extent upon solid solution hardening. Moreover, through the addition of yttrium oxide particles, the high temperature performance of MA 6000 is superior to conventional superalloys [1]. This paper reports on the microstructure of MA 6000 deformed at 760 °C and 790 °C.

Ordered Ni_3Al deforms by the glide of a pair of unit dislocations (= one superlattice dislocation), which minimizes the amount of disorder by reducing the APB. It is well known that each unit dislocation can split into two Shockley partials, a/6<112>, forming a so-called complex stacking fault (CSF). If the ratio of APB and SISF (Superlattice Intrinsic Stacking Fault) energies is high enough, a superlattice dislocation dissociates into two superlattice Shockley partials, a/3<112>, separated by an SISF as observed in Zr_3Al [2]. Now the question arises which dislocations deform a superalloy containing a high volume fraction of $L1_2$ ordered precipitates. Mobile dislocations may pass the precipitates by shearing, Orowan bowing or (cooperative) climb. These mechanisms have been the subjects of analyses which mainly consider the deformation by (pairs of) unit dislocations [3][4][5]. The resistance to dislocation motion of an alloy strengthened by 50-60 volume percent precipitates is highly influenced by the capability of unit dislocations to dissociate into partial dislocations [6]. Especially, groups of partial dislocations may create a variety of fault configurations in γ' precipitates. Subsequent partial dislocations on the same slip plane lead to annihilation or extension of faulted regions.

This paper reports upon TEM observations at 200 kV of stacking faults confined to the γ' precipitates of MA 6000 after deformation at 760 °C and 790 °C.

2. Material and Experimental Procedure

Chemical composition of MA 6000 (wt%)

Ni	Cr	W	Mo	Al	Ti	Ta	C	B	Zr	Y_2O_3
69	15	4.0	2.0	4.5	2.5	2.0	0.05	0.01	0.15	1.1

Elemental analysis using energy and wavelength dispersive X-ray techniques proved small additions of Re and Cu. MA 6000 contain columnar grains with a length of about 10 mm which share a <110> axis ± 20° [7]. The transverse grain size varies between 0.1 and 1 mm. After etching, some details are visible within the columnar grains with an optical microscope. With X-ray diffraction and TEM these details have been identified to be small angle (5°) boundaries. X-ray diffraction on powder, chemically extracted, gives evidence for the presence of yttrium aluminium oxide ($YAlO_3$) and titanium tungsten carbide (Ti,W)C. About 50 volume percent of the alloy is occupied by γ' ($L1_2$) Ni_3(Al,Ti) precipitates. The small misfit between the γ matrix and γ' precipitates causes a cuboidal shape of the large precipitates which have edge lengths of 200-300 nm. Between the cuboids a small volume fraction of γ' spheres is found with a mean diameter of 25 nm. As a consequence of the shearable γ' spheres, widely separated superlattice dislocations are found in the matrix between the cuboids in MA 6000 as received.

Test specimens are prepared with the gage length parallel to the longitudinal grain direction. The specimens contain only about three columnar grains which considerably reduced the lifetime in creep

0036-9748/85 $3.00 + .00

experiments. Fracture strain was found to be approximately 8%. 2% plastically deformed specimens have been used for TEM observations. In creep 2% plastic deformation was reached at the onset of steady state creep. Tensile ($\dot{\varepsilon} = 10^{-3} s^{-1}$) and creep (538 MPa) experiments have been performed at 760 °C and 790 °C, respectively.

At the fracture surface of some test specimens, groups of spheres are found (mean diameter 5 μm). The elemental composition of these spheres could not be distinguished from the alloy composition. Therefore, it is likely that the spheres consist of a mechanically alloyed mixture of the original powders. In figure 1 such a fracture surface is depicted. This specimen could not resist 368 MPa at 790 °C. It may be concluded that the mechanical strength of the material is considerably decreased by these spheres.

3. Deformation of γ' Strengthened Alloy

Upon tensile and creep deformation at 760 °C and 790 °C, respectively, single unit dislocations have been found in the matrix. At the γ/γ' interface small ribbons of stacking faults result from the dissociation into partial dislocations. Inside γ' precipitates superdislocations are rarely found. The main feature of the microstructure after deformation is the occurrence of stacking faults inside γ' precipitates. The faults can be divided in two groups which are depicted in figure 2. By tilting it has been established that the faults are located on two {111} planes. As a result of the <110> grain orientation, two slip systems are easily activated. Initially, the stacking faults are confined to the γ' particles which may be proved by two micrographs of the same faulted precipitate, the first with a matrix reflection and the second with a superlattice reflection [8]. As deformation proceeds, faults extend into the matrix between the precipitates. In figure 2 it can be seen that further deformation produces microtwins i.e. more than two parallel layers of stacking faults. At fracture the microtwins reach a considerable density [9]. It has been confirmed experimentally that the twins are parallel to the macroscopically visible slip lines. In addition, it has been established that the direction of the slip lines coincides with the direction of the transgranular fracture surface in both creep and tensile experiments at 760 °C.

3a. Stacking faults inside γ' precipitates

An experimental method to verify whether the faults inside γ' precipitates are CSF's or SISF's is to determine the Burgers vector of the leading dislocation of a fault. The determination of the Burgers vector has been performed with the invisibility criteria $\mathbf{g}.\mathbf{b} = 0, \pm 1/3, -2/3, 4/3$. In all cases the deviation from the Bragg reflection was taken positive ($\mathbf{s} > 0$). The results are summarized in table 1. The invisibility for $\mathbf{g}.\mathbf{b} = +4/3$ is ambiguous. Nevertheless, a comparison of fig. 3a ($\mathbf{g}.\mathbf{b} = +4/3$) with fig. 3b ($\mathbf{g}.\mathbf{b} = -4/3$) reveals a clear difference in contrast. Care was taken that on reversing $\mathbf{g}$ the deviation $\mathbf{s}$ kept the same magnitude.

TABLE 1

$\mathbf{g}.\mathbf{b}$ and $\mathbf{g}.\mathbf{R}$ analysis of the fault configuration shown in fig. 3a-3d
(i = invisible, v = visible)
The extinction criteria for a stacking fault are $\alpha = n\pi$

g	$\mathbf{g}.\mathbf{b}$ $b=a/3[11\bar{2}]$	Observation	$\alpha=2\pi\,\mathbf{g}.\mathbf{R}$ $R=a/3[11\bar{2}]$	Observation	Reference
220	4/3	i	$8/3\,\pi$	v	Fig. 3a
$\bar{2}\bar{2}0$	-4/3	v	$-8/3\,\pi$	v	Fig. 3b
$\bar{2}00$	-2/3	i	$-4/3\,\pi$	v	Fig. 3c
200	2/3	v	$4/3\,\pi$	v	Fig. 3d
$20\bar{2}$	2	v	$4\,\pi$	i	
020	2/3	v	$4/3\,\pi$	v	
$0\bar{2}0$	-2/3	i	$-4/3\,\pi$	v	

The occurrence of an $a/6[11\bar{2}]$ partial dislocation is excluded because of the (in)visibility of the leading dislocation of the fault in figures 3a, b and d.

From table 1 it may be concluded that an $a/3[11\bar{2}]$ partial dislocation creates the fault inside the γ' precipitate. By observing the outermost fringes, the intrinsic character of the faults has been proven. The dislocation-fault configuration shown in figures 3a-d is just an example from a large number with the same extinction behaviour.

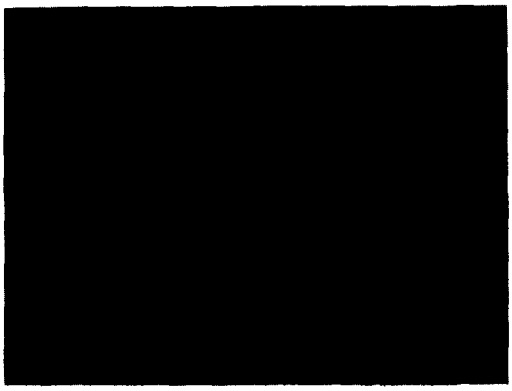

Fig. 1. Group of spheres at a fracture surface of Ma 6000.

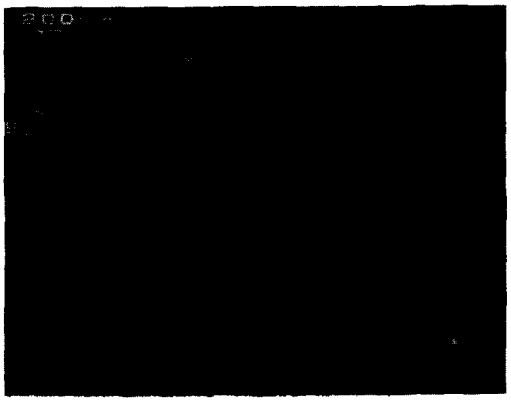

Fig. 2. Deformation induced stacking faults inside γ' precipitates.

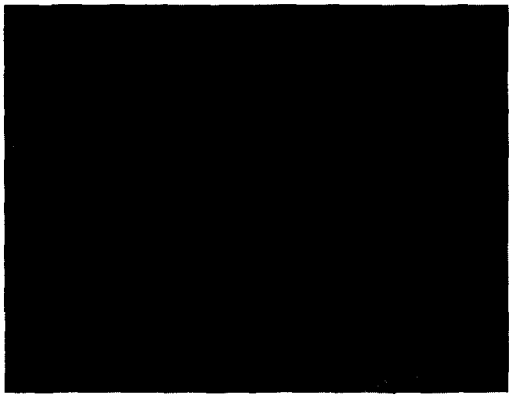

a

b

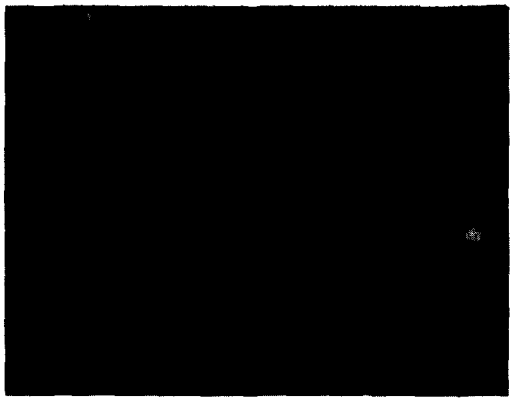

c

d

Fig. 3. a/3[11$\bar{2}$] dislocation in front of a SISF inside γ' **g.b** 1/2 4/3, -4/3, -2/3, 2/3 in figures 3a, b, c, d, respectively. (see table 1).

3b. Growth mechanism

In the previous section the faults have been identified to be of superlattice intrinsic nature. In this part the growth mechanism of these faults will be analyzed. Along the fringes of some faults a dislocation segment can be resolved. In figures 4a and 4c such a segment is visible. In figures 4b and 4c it can be seen that this fault is extended over the whole γ' precipitate. The segment seemed to be the remainder after electropolishing of a dislocation loop at the γ/γ' interface. With the invisibility criteria of section 3a, the Burgers vector was determined to be $a/6[1\bar{2}\bar{1}]$, see table 2.

TABLE 2

g.b analysis of the dislocation segment shown in figures 4a-c
(i = invisible, v = visible)

g	**g.b** b=$a/6[1\bar{2}\bar{1}]$	Observation	Reference
$0\bar{2}\bar{2}$	1	v	Fig. 4a
$\bar{2}\bar{2}0$	1/3	i	
$\bar{2}00$	-1/3	i	
$1\bar{1}\bar{1}$	1/3	i	
$\bar{2}02$	-2/3	i	
$\bar{1}11$	-2/3	i	Fig. 4b
$1\bar{1}\bar{1}$	2/3	v	Fig. 4c
$\bar{1}\bar{1}1$	0	i	

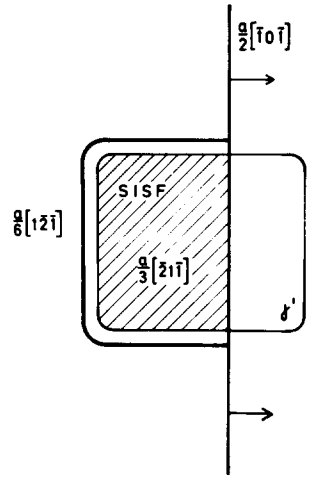

Fig. 5. Growth mechanism of stacking faults inside γ' precipitates.

Although the plane of the faults in figure 4 has been determined by tilting, the exact value of the displacement is unknown. The three possible values of R are: $a/3[\bar{2}1\bar{1}]$, $a/3[112]$ and $a/3[1\bar{2}\bar{1}]$. The third would imply that $a/2[1\bar{2}\bar{1}]$ is operative which is not the case because $a/2<112>$ partial dislocations cause other fault configurations [6]. The presence of an $a/6[1\bar{2}\bar{1}]$ loop together with $R=a/3[\bar{2}1\bar{1}]$ or $a/3[112]$ leads to the following dissociation mechanism of a unit dislocation [10]: $a/2[\bar{1}0\bar{1}] \rightarrow a/3[\bar{2}1\bar{1}] + a/6[1\bar{2}\bar{1}]$. This particular dislocation reaction is confirmed by the presence of unit dislocations which were apparently obstructed at the γ/γ' interfaces.

As depicted (schematically) in figure 5, the matrix is deformed by $a/2[\bar{1}0\bar{1}]$ whereas the precipitate is faulted by $a/3[\bar{2}1\bar{1}]$. At the γ/γ' interface an $a/6[1\bar{2}\bar{1}]$ dislocation loop is left behind. Obviously, this mechanism accounts for faults lying inside the precipitates only as experimentally observed in the first stage of deformation.

3c. Stair rod dislocations in γ' precipitates

As a result of the <110> grain orientation, two slip systems are easily activated. In the first stage of plastic deformation only one slip system is operating, but at the onset of steady state creep both systems are active. The occurrence of two slip systems causes a typical fault configuration as will be described below.

Some stacking faults (less than 1%) inside γ' precipitates reveal a line of intersection of two {111} slip planes. By edge-on tilting it was found that part A of the fault in fig. 6 is located on (111) along $[\bar{2}11]$ and part B on $(11\bar{1})$ along $[1\bar{2}\bar{1}]$. It is likely that the $a/3<112>$ partial dislocations, which have created the faults, have formed a stair rod dislocation at the line of intersection of the two slip planes. In figure 7 the stair rod dislocation is visible. Unfortunately, it was not possible to identify the Burgers vector of the stair rod dislocation with the usual invisibility criteria. If two $a/3<112>$ dislocations, one on (111) and the other on $(11\bar{1})$ react along $[\bar{1}10]$, several stair rod dislocations may be formed. Regarding the self energy, $a/3<110>$ is the most likely one.

Assuming the leading $a/3<112>$ partial dislocations which have created the faults to be of pure edge nature, the exact Burgers vector may be deduced from the direction of the faults. This implies a dislocation reaction according to $a/3[\bar{2}11] + a/3[1\bar{2}\bar{1}] \rightarrow a/3[\bar{1}\bar{1}0]$. In silicon grown-in faults have been observed with a similar stair rod dislocation [11]. The stair rod in figure 6 is one side of the triangle which reveals a contrast typical for two faults, one above another, which have a symmetrical inclination

a

b

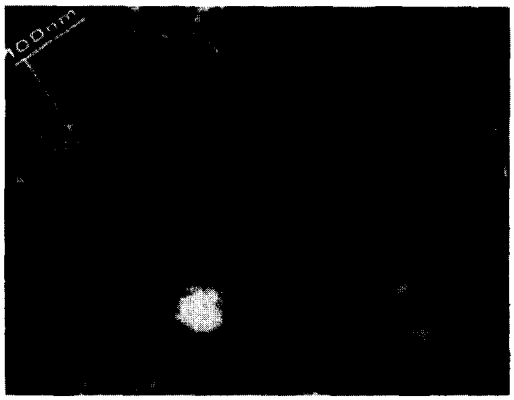

c

Fig. 4. a/6[1$\bar{2}\bar{1}$] dislocation along the fringes of a SISF. Figures a, b and c are indicated in table 2.

Fig. 6. Stacking fault inside γ'. Part A along [$\bar{2}$11] on (111). Part B along [1$\bar{2}\bar{1}$] on (11$\bar{1}$).

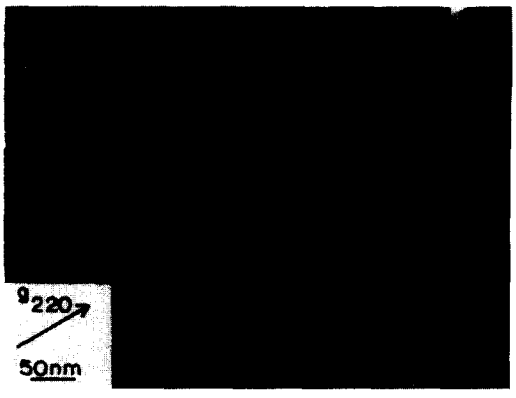

Fig. 7. A stair rod dislocation is visible along the line of intersection of the two fault planes.

to the foil as explained by Amelinckx [12]. The fringes are modulated parallel and perpendicular to the stair rod dislocation.

4. Discussion and Conclusion

After 2% tensile and creep and tensile deformation at 760 °C and 790 °C, respectively, a/3<112> partial dislocations have been identified to deform γ' precipitates. No evidence was found for a/2<112> partial dislocations. However, fault configurations typical for a/2<112> partial dislocations are observed after the first LCF experiments at 760 °C. Upon further deformation, SISF's expand in the matrix which means that the energy of an extended fault is lower than the energy of faulted precipitates separated by unfaulted matrix. The extension of faults in the matrix might be stimulated by the annihilation of interfacial Shockley dislocations.

From our results it might be concluded that upon deformation at 760 °C and 790 °C, a/3<112> partial dislocations are mobile in spite of a high Peierls stress. At room temperature deformation till fracture produces a rather low density of twins. As a matter of fact, this density is comparable with the density of twins in the as received material. Calculations show a/3<112> partial dislocations may have glissile and sessile core structures [13]. Therefore, the explanation might be that at room temperature a/3<112> partial dislocations are sessile.

The microstructure shows that superlattice dislocations coupled together by APB only play a minor role in deformation of MA 6000 at 760 °C and 790 °C. Yet a few superdislocations inside γ' precipitates are found. Measuring the distance between the two dislocations is a suitable method to obtain an estimate of the APB energy. Unfortunately, the reliability of the estimate is influenced by residual stresses. Nevertheless, the antiphase boundary energy on {111} of γ' precipitates is calculated to be 144 (± 10%) mJ/m².

In a recent paper about the so-called sawtooth faults in Ni_3Al [14], Veyssièrre has calculated that an a/3<112> partial dislocation has a stable position at a certain distance from a Shockley partial dislocation provided $\gamma_{SISF}/\gamma_{APB} < 0.1$. In MA 6000 it implies $\gamma_{SISF} < 14$ mJ/m². A spontaneous dissociation of a <110> dislocation into two a/3<112> partial dislocations has not been observed. Therefore, $\gamma_{SISF}/\gamma_{APB} > 0.03$, i.e. $\gamma_{SISF} > 4$ mJ/m². In addition Veyssièrre states that an a/3<112> may recombine with a/6<112> by thermally assisted steps. Obviously, a similar recombination of an a/3<112> with a/6<112> is necessary to account for faults in γ' precipitates by the given dissociation and recombination of a unit dislocation. The observed sawtooth in Ni_3Al and faults in γ' precipitates may be interpreted as a result of the same tendency to dissociate.

Acknowledgement

The work is part of the research program of the Foundation for Fundamental Research on Matter (F.O.M.-Utrecht) and has been made possible by financial support from the Netherlands Organization for the Advancement of Pure Research (Z.W.O.-The Hague).

References

1. R. F. Decker, 4th Int. Symposium on Superalloys, Sept. 1980.
2. L. M. Howe and M. H. Rainville, Proc. 9th Int. Congr. on Electr. Microscopy, Toronto, 1978, Vol. 1, 404 (1978).
3. B. Reppich, Acta Met. **30**, 87 (1982).
4. M. Mc Lean, Acta Met. **33**, 545 (1985).
5. R. K. Ham, Proc. 3rd Bolton Landing Conf., Sept. 1969 (Eds. B. H. Kear, C. T. Sims, N. S. Stoloff and W. H. Westbrook), 365 (1969).
6. J. M. Oblak and B. H. Kear, Electron Microscopy and Structure of Materials (Eds. G. Thomas, R. M. Fulrath and R. M. Fisher), Un. Calif. Press, 566 (1972).
7. T. E. Howson, D. A. Mervyn and J. K. Tien, Met. Trans. **11A**, 1609 (1980).
8. A. J. Huis in't Veld, P. M. Bronsveld, G. Boom, J. Th. M. De Hosson, 7th ICSMA, Montreal, Quebec (Canada), August 1985.
9. A. J. Huis in't Veld, P. M. Bronsveld, G. Boom, J. Th. M. De Hosson, Proc. 8th European Congress on Electron Microscopy, Budapest, Hungary, Aug. 13-18, Vol. 2, 851 (1984).
10. B. H. Kear, A. F. Giamei, J. M. Silcock and R. K. Ham, Scripta Met. **2**, 287 (1968).
11. H. Föll, C. B. Carter and M. Wilkens, Phys. Stat. Sol. (a) **58**, 393 (1980).
12. S. Amelinckx, Solid State Physics, Supplement 6. The Direct Observation of Dislocations, Academic Press, New York and London (1964).
13. M. Yamaguchi, V. Paidar, D. P. Pope and V. Vitek, Phil. Mag. **A 45**, No. 5, 883 (1982).
14. P. Veyssièrre, J. Douin and P. Beauchamp, Phil. Mag. **A 51**, No. 3, 469 (1985).
15. V. C. Nardone and J. K. Tien, Scripta Met. **17**, 467 (1983).